Electrochimica Acta 557 (2026) 148464

Contents lists available at ScienceDirect

Electrochimica Acta

journal homepage: www.journals.elsevier.com/electrochimica-acta

Electrochromic behavior of dimethyl terephthalate in ionic liquids-based quasi-solid matrices

Tehreema Naeem, Neus Vilà, Jordi Hernando, Gonzalo Guirado *

Departament de Química, Universitat Autònoma de Barcelona, Bellaterra (Barcelona), 08193, Spain

ARTICLE INFO

Keywords:
Electrochromic devices
Ionogels
Ionic liquids
Dimethyl terephthalate

ABSTRACT

This study reports a solid-state electrochromic device (ECD) based on dimethylterephthalate (DMT), demonstrating high stability and low operating voltage on both rigid and flexible substrates. DMT molecules were incorporated into a poly(vinylidene fluoride-*co*-hexafluoropropylene) ionogel (IG) using ionic liquids as environmentally friendly electrolytes. Cyclic voltammetry and in-situ spectroelectrochemistry were employed to investigate the electrochromic mechanism in the DMT@IG system. An ECD with two electrodes was fabricated on ITO-coated glass, operating at a low potential difference of 2 V, with bleaching times of 2.06 s, coloration times of 5.92 s, an optical contrast of 21%, and a color efficiency of 147.7 cm^2 C^{-1}. The device maintained stability for up to 30 cycles. Furthermore, a flexible three-electrode configuration with a DMT@IG membrane was designed, confirming DMT's potential as an advantageous material for low-voltage electrochromic and flexible display applications.

1. Introduction

With the growing development of smart materials and technologies, electrochromism has attracted increasing attention for applications ranging from multi-color displays and sensors to energy storage devices and smart windows [1–6]. Electrochromic devices (ECDs) rely on the same fundamental phenomenon: a reversible color change induced by an applied voltage which is accompanied by modulation of optical properties such as transmittance, reflectance, and absorbance [7–10]. Among organic electrochromic compounds (OECs), viologens and π-conjugated polymers such as polyaniline and polythiophene have been widely studied due to their high coloration efficiency, chemical stability, and reliable device performance [11–13]. To achieve full-color electrochromic displays, it is essential to develop materials capable of producing one of the three primary colors (cyan, magenta, or yellow) [14].

Compared to these well-established OECs, phthalate esters remain relatively underexplored despite their promising electrochromic potential and reported reversible color switching [15–17]. Within this family, dimethyl terephthalate (DMT) is of particular interest. DMT is a small ester-containing electrochromic (EC) molecule that undergoes a reversible transition from colorless to magenta—one of the three primary colors—upon electrochemical stimulation. This distinctive property makes DMT a promising candidate for the development of low-cost ECDs with high optical contrast and coloration efficiency [18]. However, prior studies on DMT have been limited to solution-phase systems, which suffer from poor stability, safety concerns, and electrolyte leakage issues [19].

To mitigate these challenges, gel-based polymer electrolytes have been explored, with poly(vinyl butyral) (PVB)-based systems among the most widely studied [20–24]. While this strategy effectively minimizes leakage, the use of aprotic solvents and supporting electrolytes remains a significant limitation. Conventional solvents such as dimethyl sulfoxide (DMSO) pose risks of volatility, chemical instability, and environmental hazards. In contrast, ionic liquids (ILs) have emerged as promising alternatives, offering negligible vapor pressure, low flammability, tunability, and a wide electrochemical window of up to 5 V [25–27].

In recent years, ILs have also been incorporated into polymer networks to form ionogel (IG) membranes, a new class of hybrid materials in which the polymer acts as the dispersed phase and the IL serves as the continuous phase. IGs integrate the advantageous properties of both components, providing intrinsic ionic conductivity while eliminating the need for additional supporting electrolytes [28–31]. Recent reports have demonstrated IG-based ECDs using OECs such as viologens and thiazine derivatives, achieving high coloration efficiencies and excellent cycling stability [32–34].

* Corresponding author.
E-mail address: gonzalo.guirado@uab.cat (G. Guirado).

https://doi.org/10.1016/j.electacta.2026.148464
Received 12 December 2025; Received in revised form 28 January 2026; Accepted 15 February 2026
Available online 18 February 2026

In this study, we investigate for the first time the electrochromic mechanism of DMT in solid-state electrolytes based on ILs. Electrochemical analysis of DMT were carried out in various ILs to evaluate the influence of different cation and anion combinations on DMT's redox and optical behavior: 1-ethyl-3-methylimidazolium ([EMIM]), 1-butyl-3-methylimidazolium ([BMIM]), 1-butyl-1-methylpyrrolidonium ([BMPyr]), *N*-trimethyl-*N*-butylammonium ([N_{1114}]) and 1-methyl-1-propylpiperidinium ([PP13]) as cations, and bis(trifluoromethanesulfonyl)imide ([TFSI]) and tetrafluoroborate ([BF_4]) as anions (Fig. 1, top). For the preparation of DMT-based solid-state electrolytes, ionogels composed of poly(vinylidene fluoride-*co*-hexafluoropropylene) (PVDF-co-HFP), a fluorinated copolymer, and [EMIM]TFSI were fabricated (Fig. 1, bottom). The primary objective of this work was to evaluate the electrochromic performance of DMT within IG membranes and to fabricate ECDs capable of stable and reversible color switching at low operating voltages. Key device parameters, including optical contrast, switching times, and coloration efficiency, were systematically evaluated

2. Experimental section

2.1. Materials and reagents

Dimethyl terephthalate (≥99 %) and polyvinylidene fluoride-*co*-hexafluoropropylene were purchased from Aldrich (≥99 %) and used as received. Dimethyl sulfoxide (>99 %) and Ferrocene (Fc, >98 %) were received from Fluka and used without further purification. High-purity acetonitrile (ACN) was purchased from Acros Organics (>99.5 %). Ionic liquids [BMIM][TFSI], [EMIM][TFSI], [BMPyr][TFSI], [N_{1114}][TFSI], [PP13][TFSI], and [EMIM][BF_4] were purchased from Solvionic and used without further purification.

2.2. Synthesis of electrochromic IGs

For the DMT@IG membranes formulation, a 1:5 wt ratio of PVDF-co-HFP and [EMIM][TFSI] was mixed, and 5 mL of acetone was added to the mixture. The mixture was then left to stir until all the polymer was completely dissolved (IG solution). Then, 5 mM of DMT was added to the IG solution and sonicated for 5 min to achieve homogeneity. Finally, a volume of 90 µL IG solution was poured into a polydimethylsiloxane (PDMS) template for each membrane and left to air dry for 15– 20 min . As a result, free-standing and elastic solid membranes were obtained of 1-cm of diameter and 250 µm of thickness was obtained by profilometry (see Figure SI1).

For the DMT@IG membranes that incorporate ferrocene, a 1:2 wt ratio of DMT and ferrocene was dissolved in 2 mL of IG solution and sonicated for 5 min . Then, a volume of 90 µL of IG solution was poured into the PDMS template for each membrane and left to air dry for 15– 20 min .

2.3. Fabrication of 2-electrode system and flexible displays

For ECD fabrication, commercially available indium tin oxide (ITO)-coated glasses were used as electrodes. To build up the device, a double-sided adhesive layer of 1.1 mm in thickness was used to create a 1.7 cm x 1.5 cm well on the top of an ITO-glass substrate. Then, 360 µL (4 times 90 µL, letting it dry for 20– 30 min each time) of the IG solution was dropcasted into the well. After that, 15 µL of DMSO was poured onto the membrane formed, and the device was assembled into a sandwich structure using a second ITO-glass layer. The device was gently pressed to ensure good contact with the electrodes.

Fabrication of the flexible, three-electrode electromic display required assembling five layers (1– 5): 250 µm-thick layers of poly (methyl methacrylate) (PMMA) were used as the top and bottom covers of the device (1 and 5); a 175 µm thick pressure-sensitive adhesive (PSA, 2) layer as a white background was placed on top of PMMA layer 1, which contained an engraved electrochemical cell; a 1 mm-thick PMMA layer (3) was used to connect the DropSense ITO electrode with the electrochemical cell; a 100 µm-thick, transparent PSA layer (4) was finally used to bind layers 3 and 5.

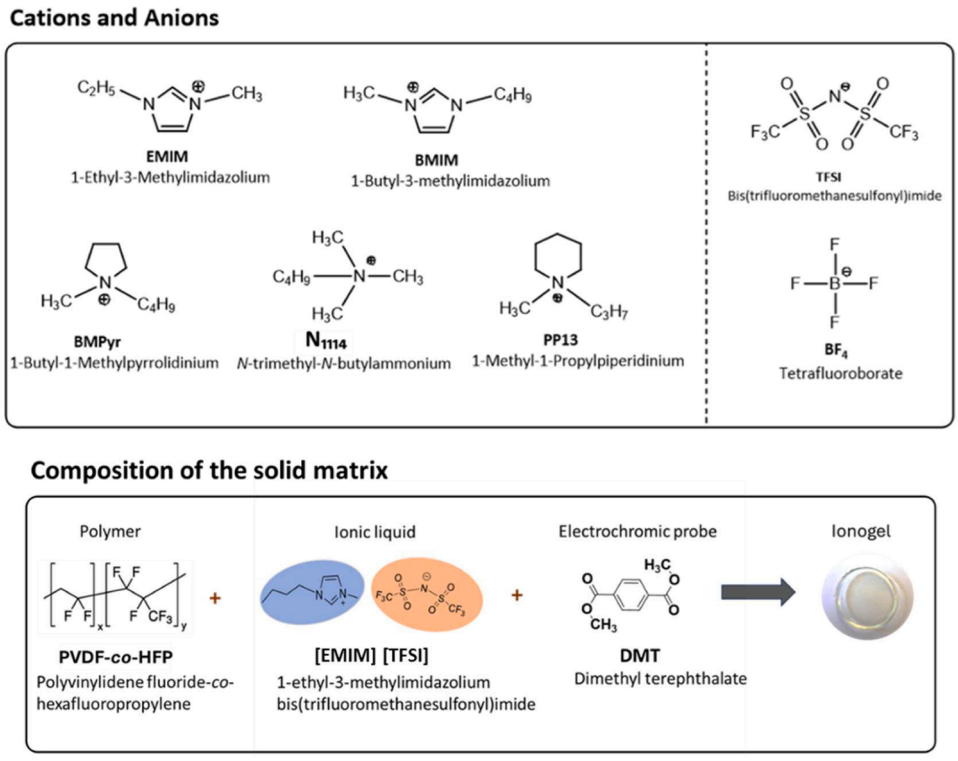

Fig. 1. (top) Chemical structures of the cations and anions of the ionic liquids used in this study. (bottom) Composition of the electrochromic ionogel membranes developed based on PVDF-co-HFP, [EMIM][TFSI] and DMT.

2.4. Characterization techniques

Cyclic voltammetry was used to measure the electrochemical potential windows of all ILs analyzed and to determine the electrochemical properties of DMT. For ILs, cyclic voltammetry experiments were performed in a three-electrode system with glassy carbon as a working electrode (WE, diameter (d) = 1 mm). A Pt disk ($d < 1$ mm) was used as a counter electrode (CE), along with a saturated calomel electrode (SCE) as the reference electrode (RE). These measurements were recorded on a 660E CHInstrument potentiostat. For DMT@IG membranes, cyclic voltammetry was performed with a commercially available three-electrode screen-printed system, which was purchased from Methrom DropSensens, using glassy carbon as WE and CE, and silver as the pseudoreference electrode.

For spectroelectrochemistry measurements, a VSP model potentiostat was used along with the EC-Lab V11.43 software. The potentiostat was synchronized with a Hamamatsu spectrophotometer to record UV–vis spectra. Bio-kine 32 V4.82 software was used to record and process absorbance data. The electrodes used in the spectroelectrochemical studies included a Pt mesh as WE, a Pt wire CE, and a SCE RE, when DMT was studied in solution. An optically transparent screen-printed electrode (DRP-ITO10) was selected for characterizing DMT in IG membranes. DRP-ITO10 contains an ITO WE, glassy carbon as CE, and silver as the pseudoreference electrode. For the two-electrodes systems, spectroelectrochemical characterization was performed with two ITO-coated glass as working and counter electrodes in a sandwich configuration.

The IG thickness was characterized by confocal imaging, which is described as a non-contact optical 3D profiling technique. The characterization was carried out by using DCM 3D optical profilometer (Leica), which was provided by UAB Microscopy Service. The IG morphology was evaluated by using a Zeiss Merlin Scanning Electron Microscope (SEM), a high-resolution field emission microscope (See Figure S12).

3. Results and discussion

To select the most suitable IL to fabricate a low-voltage electrochromic device, different ILs were first tested as liquid electrolytes, focusing on the analysis of the IL cation and anion effects on the electrochemical performance of DMT.

3.1. Electrochemical characterization of DMT in ionic liquids

3.1.1. Cation effect

The effect of IL cation on the electrochemical behavior of DMT was analyzed using five ionic liquids containing a common anion ([TFSI]) but different cations: imidazolium, piperidinium, pyrrolidinium, and ammonium. Fig. 2 shows the cyclic voltammograms of DMT in these ILs, which were recorded on a glassy carbon working electrode at various scan rates within a potential window of 0 to –2.2 V (vs SCE). In all ILs, DMT exhibited two well-defined and reversible redox processes in the cathodic region, featuring the characteristic electrochemical parameters summarized in Table 1.

The redox potentials of DMT reduction waves were found to be independent of scan rate, suggesting that the associated redox processes are thermodynamically controlled. Across all ILs, DMT exhibited analogous electrochemical behavior with only minor changes in peak potentials. In each case, two sequential monoelectronic and reversible electron transfer processes were observed. Based on these results, a two-step reduction mechanism was proposed: formation of the DMT radical anion upon the first electron transfer, followed by the formation of a dianion upon the second reduction (Fig. 3).

The differences observed in the CV peak currents and potentials across the various ionic liquids— [EMIM]TFSI, [BMIM]TFSI, [BMPyr]TFSI, [PP13]TFSI, and [N1114]TFSI—arise from their distinct physicochemical properties. These ILs span a wide range of viscosities, cation sizes, and microstructural organization, all of which strongly influence mass transport and electron-transfer kinetics. Lower-viscosity imidazolium ILs ([EMIM]TFSI, [BMIM]TFSI) provide faster diffusion and higher peak currents, whereas bulkier pyrrolidinium, phosphonium, or ammonium cations ([BMPyr]TFSI, [PP13]TFSI, [N1114]TFSI) slow ion mobility, leading to reduced corrents, To reliably compare the electrochemical responses across these ILs, the parameter $I_p/(c\nu^{1/2})$ was used to normalize the peak currents, allowing the intrinsic IL-dependent transport behavior to be evaluated [34,35].

Focusing on the potential values, the first reduction process of DMT was found to be highly reversible across all ILs, showing negligible differences in the formal potential (E^o) for all liquid electrolytes considered. In contrast, the second reduction potential exhibited a pronounced dependence on the nature of the cationic species of the IL. Specifically, in imidazolium-based ILs ([EMIM][TFSI] and [BMIM][TFSI]), both the cathodic peak potential (E_{pc}) and E^o were shifted toward more positive values compared to the other ILs (ca. 100 mV). This shift suggests stronger solvation of DMT in imidazolium ILs, likely due to specific ion-pairing effects [34,35]. The aromatic structure of imidazolium cations enables π–π interactions with DMT, while hydrogen bonding between the carbonyl oxygen atoms of DMT and the acidic proton at C2 position of imidazolium ions may further stabilize the reduced species. In contrast, aliphatic cations such as [N_{1114}], [BMPyr], and [PP13] lack aromaticity and acidic hydrogens, resulting in weaker cation-solute interactions and consequently poorer solvation of DMT [35]. Notably, the electrochemical response of DMT in [EMIM][TFSI] and [BMIM][TFSI] was nearly identical, indicating that the bulkier alkyl substituent in [BMIM] has minimal influence on solvation environment and overall redox characteristics. After analyzing all these results, we concluded that the ILs containing imidazolium cations are better for fabricating DMT@IG membranes.

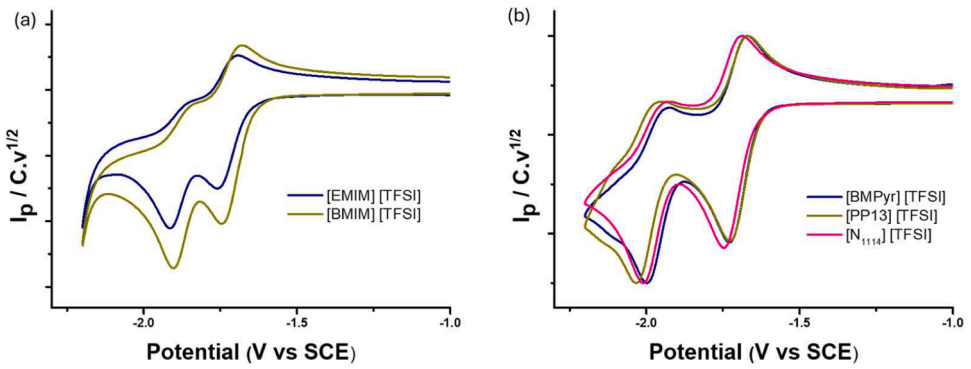

Fig. 2. Cyclic voltammograms of 50 mM DMT in (a) [EMIM][TFSI] and [BMIM][TFSI], and (b) [BMPyr][TFSI], [N_{1114}][TFSI], and [PP13][TFSI] (WE: glassy carbon, CE: Pt, and RE: SCE; scan rate: 0.1 V s^{-1}).

Table 1
Electrochemical features of DMT reduction waves in TFSI-based ILs bearing different cations.[a].

IL	$E_{pc,1}$ (V)	$E_{pa,1}$ (V)	ΔE_{p1}[a] (mV)	E^0_1(V)	$E_{pc,2}$ (V)	$E_{pa,2}$ (V)	ΔE_{p2}[a] (mV)	E^0_2 (V)
[EMIM] TFSI	−1.76	−1.69	70	−1.73	−1.91	−1.85	60	−1.88
[BMIM] TFSI	−1.75	−1.68	70	−1.71	−1.90	−1.85	50	−1.88
[BMPyr] TFSI	−1.73	−1.67	60	−1.69	−1.99	−1.92	70	−1.84
[PP13] TFSI	−1.73	−1.67	60	−1.69	−2.03	−1.96	70	−1.99
[N_{1114}] TFSI	−1.75	−1.69	60	−1.72	−2.01	−1.93	80	−1.97

[a] Cathodic (E_{pc}) and anodic (E_{pa}) peak potentials, standard potential (E^0), and peak-to-peak separation ($\Delta E_p = E_{pc} - E_{pa}$) for the two reduction waves of DMT.

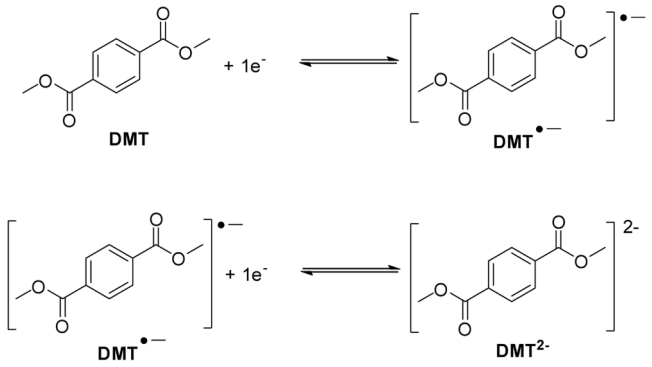

Fig. 3. Electrochemical reduction mechanism proposed for DMT in the ILs under study.

3.1.2. *Anion effect*

To investigate the role of the IL anion on DMT electrochemistry, [EMIM][TFSI] and [EMIM][BF_4], which share the same imidazolium cation, were analyzed as liquid electrolytes. CV measurements showed that two reversible redox processes are observed for DMT in both ILs, irrespective of the anion (Fig. 4 and Table 2). However, a clear difference in potential values was found, with both redox waves in [EMIM][BF_4] shifted positively by nearly 100 mV compared to [EMIM][TFSI] (Table 2). This potential shift indicates that the anion strongly influences the solvation environment and contributes to the stabilization of the reduced DMT species.

The differences observed between [EMIM][TFSI] and [EMIM][BF_4] arise from their distinct viscosities, ion sizes, and specific interactions with DMT, which directly affect diffusion and electron-transfer kinetics. The smaller and less viscous [EMIM][BF_4] enables faster mass transport and more reversible CV behavior, whereas the larger, more viscous $TFSI^-$ medium slows diffusion, resulting in lower currents and broader, shifted peaks. Peak currents were normalized using $I_p/(c\nu^{1/2})$, as previously mentioned, to allow a fair comparison between ionic liquids with intrinsically different transport properties.

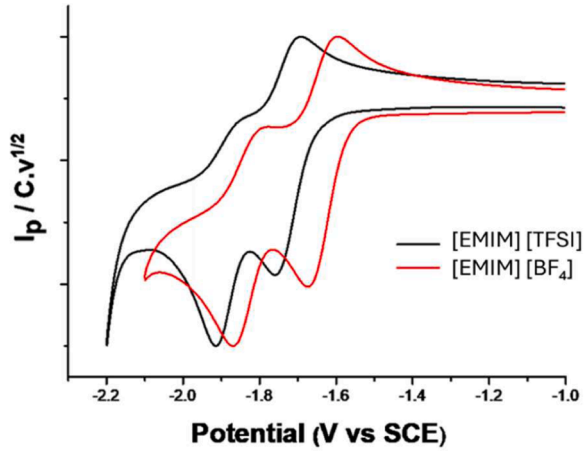

Fig. 4. Cyclic voltammograms of 50 mM DMT in [EMIM][TFSI] and [EMIM][BF_4] (WE: glassy carbon, CE: Pt, and RE: SCE; scan rate: 0.1 V s^{-1}).

In this sense, the smaller [BF_4] anion can approach the electrode surface more closely, thereby facilitating electron transfer, whereas the steric bulk and charge delocalization of [TFSI] keep it farther from the interface [36]. An additional effect to consider is the so-called umbrella effect. In the presence of [TFSI], the [EMIM] cation becomes more sterically shielded, limiting its ability to directly interact with DMT. This steric hindrance weakens potential π–π stacking and hydrogen bonding between [EMIM] and $DMT^{\bullet-}$, thus requiring more negative potentials for electron transfer. By contrast, with [EMIM][BF_4], the smaller anion does not impose such steric shielding, leaving [EMIM] more accessible for interaction with DMT, which favors reduction at less negative potentials [37] .

Despite the favorable potential shifts observed with [EMIM][BF_4], this IL suffers from drawbacks such as hydrolytic instability and possible HF generation under ambient conditions, which compromise its practical application in device fabrication [38]. In contrast, [EMIM][TFSI], though leading to slightly more negative potentials, provides superior chemical robustness, a wider electrochemical stability window, and lower environmental risks. For these reasons, [EMIM][TFSI] was chosen as the most optimal medium for the preparation of ionogel membranes and subsequent electrochromic device fabrication.

3.2. *Spectroelectrochemical characterization of DMT in [EMIM][TFSI]*

In-situ spectroelectrochemistry experiments were carried out to gain deeper insight into the electrochromic response of DMT and to verify the reduction mechanism established by cyclic voltammetry. Based on the CV data measured for DMT in [EMIM][TFSI], two potentials were chosen to probe the color changes occurring upon successive reduction steps. It must be noted that parent DMT is colorless, as it does not significantly absorb in the visible region. When a potential of –1.8 V (vs SCE) was applied, an absorption band appeared at around 530 nm, which is attributed to the formation of the radical anion $DMT^{\bullet-}$, leading to characteristic magenta coloration. Increasing the applied potential up to –2.0 V (vs SCE) to promote the second reduction process of DMT, resulted in a further enhancement in the intensity of the absorption in the visible region, consistent with the generation of the dianion DMT^{2-} (Fig. 5). Since both reduced species give rise to similar absorption bands, the chromophore responsible for the magenta color must already be established after the first electron transfer, while the second electron transfer essentially enhances the overall optical density. When the potential was returned to 0 V (vs SCE), the sample fully bleached and the absorption spectrum recovered to its original state, confirming the reversibility of DMT's electrochromic switching. A gradual fading of the reduced species was also observed, which can likely be attributed to the relatively high viscosity of [EMIM][TFSI] slowing down diffusion away from the electrode surface.

3.3. *Electrochromism of DMT in ionogel membranes*

After establishing the electrochromic behavior of DMT in [EMIM][TFSI] solution, IG membranes were prepared by mixing [EMIM][TFSI], PVDF-co-HFP and DMT to analyze the electrochromic response in a

Table 2
Electrochemical features of DMT reduction waves in EMIM-based ILs bearing different anions.[a].

IL	$E_{pc,1}$ (V)	$E_{pa,1}$ (V)	ΔE_{p1} (mV)[a]	E_1^0 (V)	$E_{pc,2}$ (V)	$E_{pa,2}$ (V)	ΔE_{p2} (mV)[a]	E_2^0 (V)
[EMIM] TFSI	−1.76	−1.69	70	−1.73	−1.91	−1.85	60	−1.88
[EMIM] BF_4	−1.69	−1.61	80	−1.65	−1.89	−1.81	80	−1.85

[a] Cathodic (E_{pc}) and anodic (E_{pa}) peak potentials, standard potential (E^0), and peak-to-peak separation ($\Delta E_p = E_{pc} - E_{pa}$ for the two reduction waves of DMT.

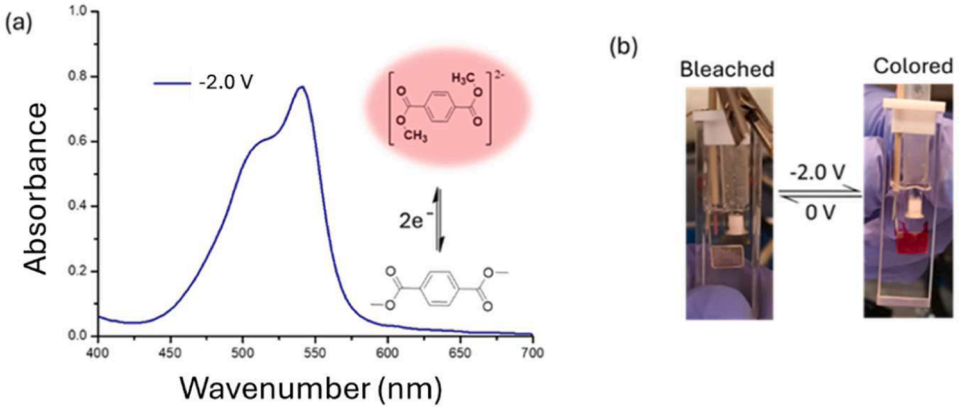

Fig. 5. (a) UV– vis absorption spectrum of 5 mM DMT in [EMIM][TFSI] at an applied potential of −2.0 V. (b) Photographs of the spectroelectrochemical 3-electrode cell (WE: Pt mesh, CE: Pt wire, and RE: SCE), showing reversible electrochromic behavior of DMT from colorless to magenta upon application of reduction voltages in [EMIM][TFSI].

quasi-solid medium. The fluorinated copolymer PVDF-co-HFP was chosen as matrix for IG preparation because of the good results previously obtained by us for the fabrication of other electrochromic devices [39–41]. Two different experimental configurations were employed to test the electrochromic performance of the resulting DMT-loaded IGs: (i) a three-electrode flexible device, and (ii) a two-electrode sandwich configuration.

3.3.1. Flexible electrochromic system based on DMT-containing ionogel membranes

To demonstrate the potential of DMT-based flexible electrochromic displays for smart device applications, a flexible device incorporating DMT@IG membranes was fabricated. A three-electrode electrochemical system was constructed using an ITO screen-printed electrode as WE. A 1 cm-in-diameter DMT@IG membrane was placed on top of this electrode and then inserted into the 5-layered electrochemical setup. Thanks to the flexibility of all components - the ionogel membrane, the screen-printed electrode, and the electrochemical cell - the electrochromic response of the resulting system could be investigated both in flat and bent configurations.

Fig. 6a compares the cyclic voltammetry responses recorded in the straight and bending states of the device to induce the electrochromic behaviour of DMT. Consistent with results previously obtained in ionic liquid solutions, the cyclic voltammogram of DMT displays two reversible reduction waves. A comparable electrochemical response is observed under bending conditions, indicating that mechanical deformation does not affect its redox behaviour. However, as expected for solid media, these waves are less defined than they are in solution. This can be attributed to the solid nature of the matrix, in which ion diffusion is slower. Nevertheless, the peaks were sufficiently separated for analysis of the cyclic voltammogram. Optical characterization was additionally carried out in both device states, showing comparable optical contrast values for the straight and bent configurations (Fig.SI3).

Notably, a redox-induced color change from colorless to magenta was observed at an applied voltage of −2,0 V (vs SCE), representing the reversible transformation of DMT into $DMT^{\bullet-}$ and DMT^{2-}. The demonstrated flexible display (Fig. 6b) represents the possibilities for using DMT in smart electronics such as smart windows, wearable displays, and reflective devices [19].

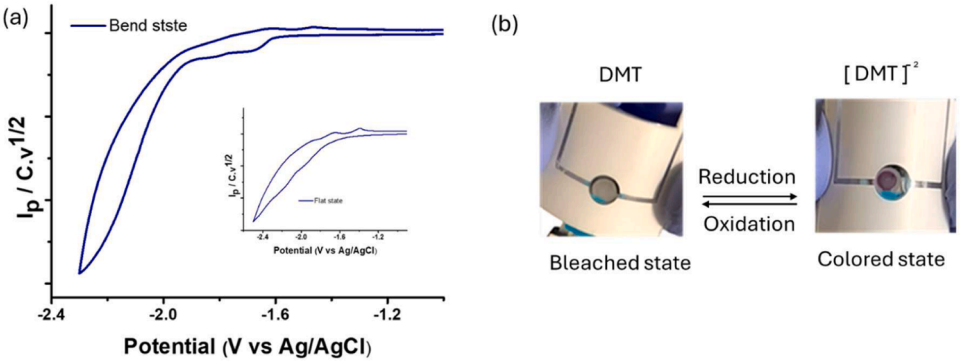

Fig. 6. (a) cyclic voltammogram of DMT@IG membranes deposited onto a screen-printed ITO electrode (CE: glassy carbon; RE: Ag; scan rate = 0.1 mV s^{-1}) in bent configurations. *(inset)* CV of DMT@IG membranes in flat configuration. (b) Flexible, three-electrode display exhibiting the reversible electrochromism of DMT in IG membranes.

3.3.2. Electrochromic device based on DMT-containing ionogel membranes

Once demonstrated that it is possible to obtain the redox response of the DMT into IG membranes, a larger, two-electrode electrochromic device was fabricated using ITO-coated glass electrodes in a sandwich configuration (Fig. 7).

Initially, an applied potential of approximately 6 V was required to induce a color change in the resulting DMT@IG-based ECD. However, the membrane was damaged after just one cycle due to the high voltage used (Fig. 8). This high operating voltage was attributed to the absence of a counter electrode reaction in the two-electrode configuration [42]. To counterbalance the reductive behavior of DMT and lower the operating voltage of the EC device, several redox mediators were introduced to provide a complementary counter electrode reaction.

Four mediators, including tetrathiafulvalene (TTF), 2,2,6,6-tetramethylpiperidine-1-oxyl (TEMPO), hexaammineruthenium(II) chloride ($[Ru(NH_3)_6]Cl_2$), and ferrocene (Fc), were evaluated individually. Such mediator were chosen to ensure optical transparency (in the case of ferrocene especially at low concentrations) in both redox states, good compatibility with the ionogel matrix, and low operating voltages. This design strategy enables a balanced optimization of electrochemical stability, optical performance, and overall device durability. For each mediator, and after some preliminary experiments, the IG membranes were fabricated with an optimal 1:2 DMT: mediator weight ratio. It was crucial to determine the optimal membrane composition for achieving the best performance of the EC device, while maintaining a low operating voltage and achieving as much color neutrality as possible in the initial state, along with device stability.

Incorporation of TTF decreased the operating voltage to 1.9 V from the initial 6 V. However, the device exhibited poor cycling stability, losing reversibility after two cycles. This lack of robustness was attributed to weak electronic coupling between TTF and DMT and to the intrinsic yellow coloration of TTF, which led to nonuniform optical transitions. Similarly, although the use of TEMPO reduced the operating voltage to 3.7 V, the electrochromic response was limited to a single cycle. Subsequent irreversible browning of the membrane was associated with TEMPO overoxidation, consistent with its limited stability at high potentials [43,44]. These results highlight the need for precise redox compatibility when selecting organic mediators.

By adding the inorganic redox mediator $[Ru(NH_3)_6]Cl_2$, the operating voltage of the ECD decreased down to 3.4 V (DMT-Ru@IG-based ECD). The mediator provided color neutrality, enabling a clear and reversible transition between bleached and colored states. Nevertheless, the operating voltage remained relatively high, limiting its suitability for low-voltage applications. Finally, we tested Fc as a mediator (DMT-Fc@IG-based ECD), whose incorporation into the device further decreased the operating voltage down to 2.0 V, consistent with the standard potentials of DMT (−1.73 V vs SCE) and Fc (0.4 V vs SCE). Under these conditions, reversible electrochromism was achieved with a robust optical response. Mechanistically, DMT was reduced at the cathode to its DMT dianion form after two electron transfer processes, producing a yellow–pink coloration. This color originated from the combination of Fc's inherent yellow hue and the magenta color of DMT^{2-}, reflected in the appearance of a new band at 530 nm in the UV–vis absorption spectrum. Concurrently, Fc was oxidized at the anode to Fc^{+}. Upon returning the applied potential to 0 V, DMT dianion was efficiently reconverted to neutral DMT, restoring the bleached state (Fig. 9a).

Overall, Fc proved to be the most effective mediator, significantly lowering the driving voltage while enhancing reversibility and optical contrast. In contrast, TTF and TEMPO were limited by poor stability and undesirable coloration, while $[Ru(NH_3)_6]Cl_2$ improved reversibility but operated at relatively high potentials. These findings highlight the crucial role of mediator selection in enabling low-voltage, stable electrochromic devices based on DMT@IG.

3.3.3. Performance of electrochromic devices based on DMT-containing ionogel membranes

Combined UV– vis absorption spectroscopy and chronoamperometry measurements were conducted to investigate the electrochromic performance of the optimal DMT-Fc@IG ECDs. For comparison purposes, the same experiments were performed on DMT-Ru@IG based ECDs.

The optical contrast achieved during redox operation of these devices was obtained from the difference in transmittance at 530 nm for their bleached and colored states ($\Delta T\%$). In case of DMT-Ru@IG-based ECDs, transmittance at 530 nm decreased from 78 % to 62 % upon coloration under 3.4 V, yielding an optical contrast of 16 % (Fig. 10). For DMT-Fc@IG-based ECDs, a larger $\Delta T\%$ value of 21 % was obtained by applying a lower coloration voltage of 2.0 V (Fig. 11). Aside from the overall optical contrast achieved, fast response times are also crucial for ECDs when considering their use in practical applications. In this study, we calculated the response time as the time that ECD needs to reach 90 % of the maximum transmittance change at 530 nm. For both Ru@IG and DMT-Fc@IG-based devices, fast response times were measured for the bleaching (t_b) and coloration processes (t_c), which fall well below 10 s: $t_b = 4.3$ s and 2.1 s, and $t_c = 6.5$ s and 5.9 s for the ECDs doped with $[Ru(NH_3)_6]Cl_2$ and Fc mediators, respectively (Fig. 10b, Fig. 11b and Table 3).

Two other parameters were investigated to assess the electrochromic behavior of the ECDs prepared. Color efficiency (CE) is a significant factor when considering ECD performance. It is measured as the ratio of the change in optical density to the charge inserted [45]. CEs at 530 nm for the DMT-Ru@IG- and DMT-Fc@IG-based devices were estimated to be 264 cm^2/C and 147 cm^2/C (Table 3), which can be considered good-to-excellent coloration performances. Finally, cyclic stability provides excellent proof of the durability and execution of an ECD, especially when considered for long-term applications. The variation in

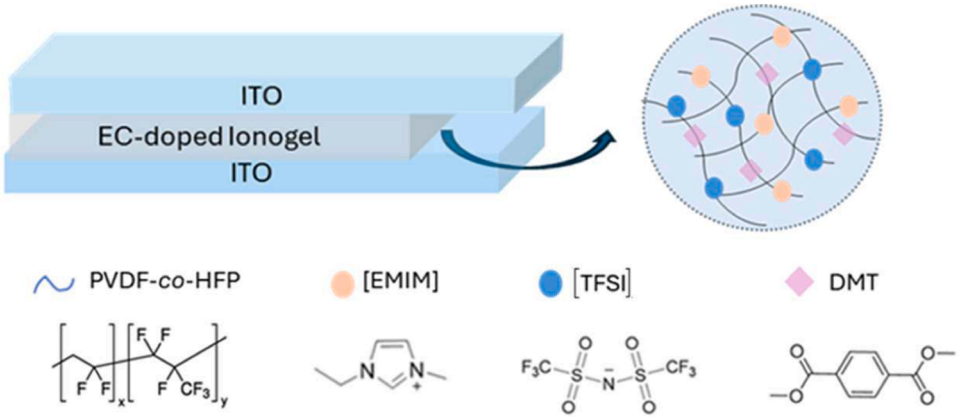

Fig. 7. Schematic representation of the composition of the two-electrode electrochromic device.

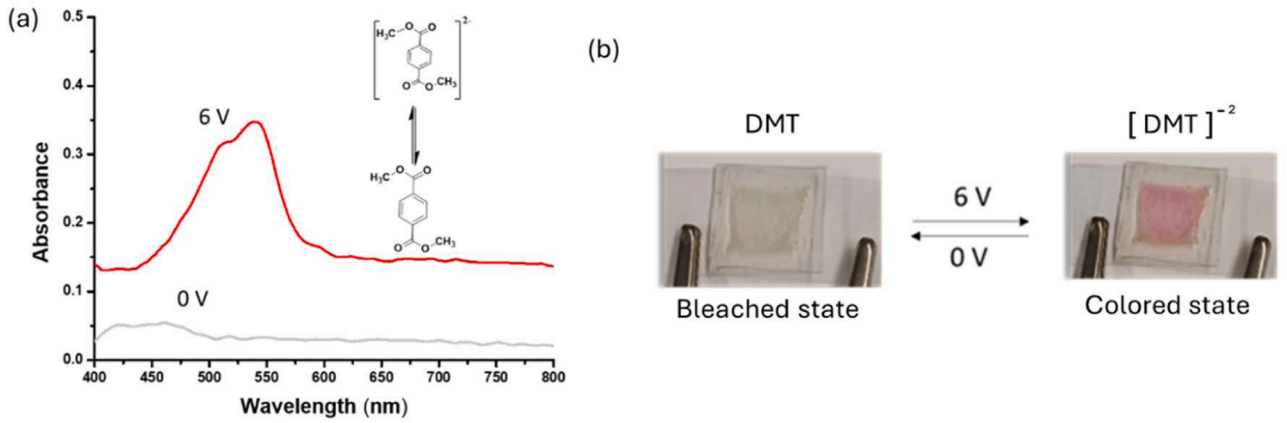

Fig. 8. (a) UV– vis absorption spectra measured at 0 V and 6 V for the two-electrode ECD in the absence of redox mediators. (b) Images of the colors achieved in this DMT-based device at the two potentials applied.

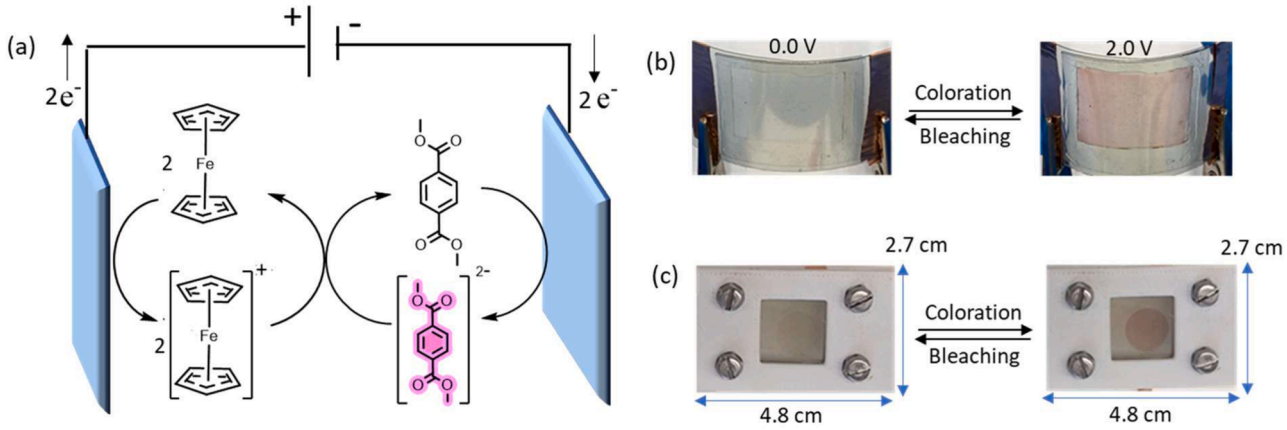

Fig. 9. (a) Schematic representation of DMT/Fc-based electrochemical cell representing the reaction mechanism originating the electrochromic response in the 2-electrode ECD. (b) Flexible display of DMT/Fc based EC device. (c) Rigid display of DMT/ Fc based EC device.

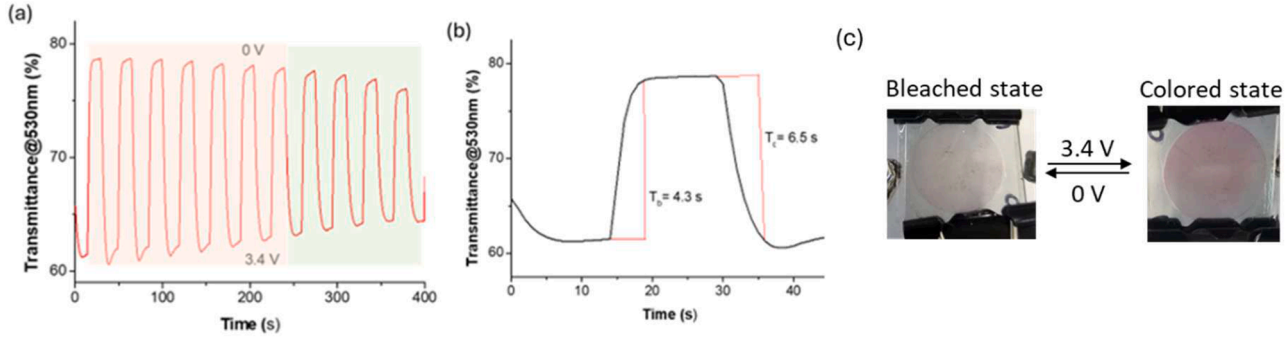

Fig. 10. (a) Transmittance switching cycles at 530 nm achieved for a DMT-Ru@IG-based ECD operated at coloration and bleaching potentials of 3.4 V and 0 V, respectively. (b) Coloration and bleaching response times for a DMT-Ru@IG-based ECD. (c) Photographs of a DMT-Ru@IG-based ECD in the bleached and colored states.

transmittance of ECDs upon sequential color switching cycles were monitored to determine their stability. In case of DMT-Ru@IG-based devices, the potential was switched between reduction and oxidation sweeps for 30 s from 3.4 V to 0 V. The reversible electrochromism of the device was observed up to 12 cycles, after which we started to observe some degradation of the response that we attribute to the high operating voltage likely inducing over-reduction processes and electrolyte instability, together with the limited solubility of the Ru-based complex in IG solution (Fig. 10a and Table 3). For the cycling test of DMT-Fc@IG-based ECDs, the potential was switched between reduction and oxidation sweeps for up to 25 cycles from 2 V to 0 V., observing good optical contrast (Fig. 11a and Table 3). To study the memory effect of the device, the device was kept in static bias condition after applying the reduction potential of 2 V. The color was observed for more than one minute, which represents the fast ionic mobility and electron transfer in the IG network even in open-circuit conditions. After that, a slight degradation was observed in the color of the membrane from light yellow to light brown, which could be ascribed to the overoxidation of

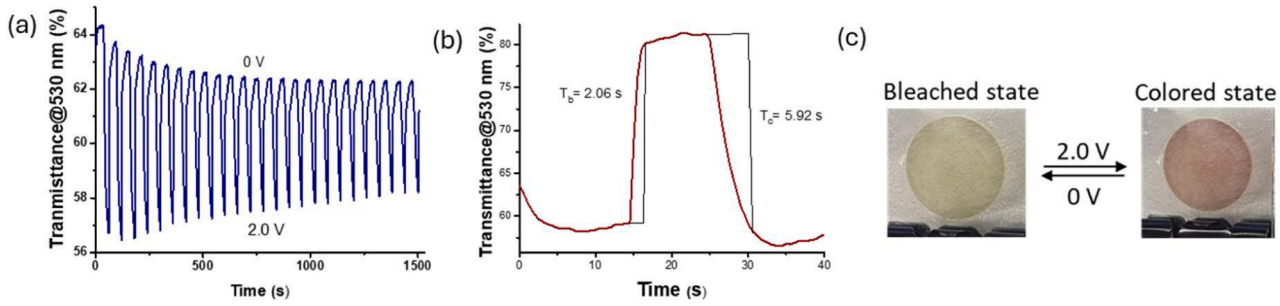

Fig. 11. (a) Transmittance switching cycles at 530 nm achieved for a DMT-Fc@IG-based ECD operated at coloration and bleaching potentials of 2.0 V and 0 V, respectively. (b) Coloration and bleaching response times for a DMT-Fc@IG-based ECD. (c) Photographs of a DMT-Fc@IG-based ECD in the bleached and colored states.

Table 3
Comparative analysis of the performance of DMT-Ru@IG- and DMT-Fc@IG-based ECDs.

Mediator	Coloration voltage (V)	Cycling stability	Response time (s)[a]	Coloration efficiency ($cm^2\ C^{-1}$)
$[Ru(NH_3)_6]Cl_2$	3.4	Up to 12 cycles	t_b= 4.5 s, t_c=6.6s	264
$Fe(C_5H_5)_2$	2.0	Up to 20 cycles	t_b= 7.9 s, t_c=5.7s	147

[a] Bleaching (t_b) and coloration (t_c) times needed to reach 90 % of the overall color change.

ferrocene due to its lower standard potential relative to DMT. To check the stability of this device, it was stored for weeks under no specific conditions without losing its electrochromic behavior (Figure S14). This result demonstrated that the device is robust under ambient conditions and does not require any specific environment for storage (Figure S15).

When compared to DMT-based devices reported in the literature using liquid electrolytes, our optimal solid-state DMT-Fc@IG-based ECD presented comparable and satisfactory electrochromic performance. Thus, Watanabe et al. reported that DMT gel-based electrochemical cells made from DMSO and NMP liquid electrolytes had to be operated at 2.3 V, exhibiting CEs of 169 and 135 cm^2/C, respectively [46]. Relative to these precedents, our IG-based devices show several advantages because of their solid-state nature, such as reducing the need to use conventional solvents and electrolytes, making them more suitable for practical electrochromic display applications.

4. Conclusions

In summary, we demonstrated the electrochromic behavior of DMT in a stable and low-operating-voltage solid-state device incorporating IG membranes, utilizing ILs as the electrolyte. We first focused on different ILs to evaluate the influence of their cation and anion on the electrochemical behavior of DMT. In particular, we studied their effect on the redox potential values of the electrochromic probe to select the IL that offered the lowest E_{pc} value and has the least toxic environmental effect. [EMIM][TFSI] was selected as the most optimal IL to synthesize IG membranes. After that, a solid-state ECD was fabricated and characterized to investigate its electrochromic performance. After adding ferrocene as a redox mediator, DMT exhibited a reversible color change from yellowish to magenta on application of coloration and bleaching voltages of 2.0 V and 0 V. Under these conditions, a 21 % change in transmittance in the visible region was achieved, which fast response times for both coloring (6.9 s) and bleaching processes (2.1 s), high coloration efficiency (147.7 cm^2/C), and switching stability over 25 cycles. These results suggest that phthalate-based electrochromic solid-state devices show high promise for the design of new sustainable smart technologies and applications.

Data availability

The data analyzed during the current study are available from the corresponding author.

CRediT authorship contribution statement

Tehreema Naeem: Writing – original draft, Validation, Methodology, Investigation. **Neus Vilà:** Writing – original draft, Methodology, Investigation. **Jordi Hernando:** Writing – review & editing, Writing – original draft, Supervision, Funding acquisition. **Gonzalo Guirado:** Writing – review & editing, Writing – original draft, Supervision, Resources, Funding acquisition, Conceptualization.

Declaration of competing interest

The authors declare that there are no conflicts to declare.

Acknowledgments

The authors thank the Ministerio de Ciencia e Innovación of Spain for financial support through project PID2022-141293OB-I00. In addition, we also acknowledge financial support from AGAUR (Generalitat de Catalunya) through project 2021 SGR 00064 and 2021 SGR 00052 as well as T. N. FI-SDUR doctoral fellowship.

Supplementary materials

Supplementary material associated with this article can be found, in the online version, at doi:10.1016/j.electacta.2026.148464.

References

[1] M.A. Farahmand Nejad, S. Ranjbar, C. Parolo, E.P. Nguyen, R. Álvarez-Diduk, M. R. Hormozi-Nezhad, A. Merkoçi, Electrochromism: an emerging and promising approach in (bio)sensing technology, Mater. Today 50 (2021) 476–498, https://doi.org/10.1016/j.mattod.2021.06.015.
[2] P.R. Somani, S. Radhakrishnan, Electrochromic materials and devices: present and future, Mater. Chem. Phy. 77 (2002) 117–133, https://doi.org/10.1016/S0254-0584(01)00575-2.
[3] R.J. Mortimer, Electrochromic materials, Chem. Soc. Rev. 26 (1997) 147, https://doi.org/10.1039/cs9972600147.
[4] P. Yang, P. Sun, W. Mai, Electrochromic energy storage devices, Mater. Today 19 (2016) 394–402, https://doi.org/10.1016/j.mattod.2015.11.007.
[5] G. Yang, Y.M. Zhang, Y. Cai, B. Yang, C. Gu, S.X.A. Zhang, Advances in nanomaterials for electrochromic devices, Chem. Soc. Rev. 49 (2020) 8687–8720, https://doi.org/10.1039/d0cs00317d.
[6] K. Lin, C. Wu, X. Wang, G. Hua, Q. Chen, S. Yan, X. Kuang, H. Liu, Y. Wang, Truxene-based multisite-polymerized electrochromic polymers: multicolor variation, excellent cycling stability, and flexible devices, Sol. Energ. Mater. Sol. Cel. 293 (2025) 113871, https://doi.org/10.1016/j.solmat.2025.113871.
[7] G. Cai, A.L.S. Eh, L. Ji, P.S. Lee, Recent advances in electrochromic smart fenestration, Adv. Sustain. Syst. 1 (2017) 201700074, 10.1002/adsu.201700074.
[8] M. Zhu, B. Xu, T. He, A.Y. Elezzabi, W. Zhang, W.W. Yu, J. Chen, Smart electrochromic devices for wearables, Adv. Mater. Technol. 10 (2025) e01015, https://doi.org/10.1002/admt.202501015.

[9] C. Gu, A.B. Jia, Y.M. Zhang, S.X.A. Zhang, Emerging electrochromic materials and devices for future displays, Chem. Rev. 122 (2022) 14679–14721, https://doi.org/10.1021/acs.chemrev.1c01055.
[10] J. Kim, M. Rémond, D. Kim, H. Jang, E. Kim, Electrochromic conjugated polymers for multifunctional smart windows with integrative functionalities, Adv. Mater. Technol. 5 (2020) 1900890, https://doi.org/10.1002/admt.201900890.
[11] T. Sagara, H. Tahara, Redox of Viologen for powering and coloring, Chem. Record 21 (2021) 2375–2388, https://doi.org/10.1002/tcr.202100082.
[12] P.M. Beaujuge, J.R. Reynolds, Color control in π-conjugated organic polymers for use in electrochromic devices, Chem. Rev. 110 (2010) 268–320, https://doi.org/10.1021/cr900129a.
[13] K. Lin, C. Wu, Y. Zhou, J. Li, X. Chen, Y. Wang, B. Lu, A multicolored polymer for dynamic military camouflage electrochromic devices, Sol. Energ. Mater. Sol. Cel. 278 (2024) 113180, https://doi.org/10.1016/j.solmat.2024.113180.
[14] Y. Alesanco, A. Viñuales, J. Palenzuela, I. Odriozola, G. Cabañero, J. Rodriguez, R. Tena-Zaera, Multicolor electrochromics: rainbow-like devices, ACS. Appl. Mater. Interfaces. 8 (2016) 14795–14801, https://doi.org/10.1021/acsami.6b01911.
[15] Y. Shi, Q. Chen, J. Zheng, C. Xu, Electrochromism of substituted phthalate derivatives and outstanding performance of corresponding multicolor electrochromic devices, Electrochim. Acta 341 (2020) 136023, https://doi.org/10.1016/j.electacta.2020.136023.
[16] P. Zhang, X. Xing, Y. Wang, I. Murtaza, Y. He, J. Cameron, S. Ahmed, P.J. Skabara, H. Meng, Multi-colour electrochromic materials based on polyaromatic esters with low driving voltage, J. Mater. Chem. C. Mater. 7 (2019) 9467–9473, https://doi.org/10.1039/c9tc02919b.
[17] W. Sharmoukh, K.C. Ko, S.Y. Park, J.H. Ko, J.M. Lee, C. Noh, J.Y. Lee, S.U. Son, Molecular design and preparation of bis-isophthalate electrochromic systems having controllable color and bistability, Org. Lett. 10 (2008) 5365–5368, https://doi.org/10.1021/ol802208x.
[18] W. Sharmoukh, K.C. Ko, J.H. Ko, H.J. Nam, D.Y. Jung, C. Noh, J.Y. Lee, S.U. Son, 5-Substituted isophthalate-based organic electrochromic materials, J. Mater. Chem. 18 (2008) 4408–4413, https://doi.org/10.1039/b808638a.
[19] H. Urano, S. Sunohara, H. Ohtomo, N. Kobayashi, Electrochemical and spectroscopic characteristics of dimethyl terephthalate, J. Mater. Chem. 14 (2004) 2366–2368, https://doi.org/10.1039/b406093h.
[20] H. Tsutsumi, Y. Nakacawa, K. Miyazaki, M. Morita, Y. Matsuda, Polymer gel films with simple organic electrochromics for single-film electrochromic devices, Poly. Chem. 30 (1992) 1725–1729, https://doi.org/10.1002/pola.1992.080300825.
[21] H. Tsutumi, Y. Nakagawa, K. Miyazaki, M. Morita, Y. Matuda, Single polymer gel Fim electrochromic device, Electrochem 37 (1992) 369–370, https://doi.org/10.1016/0013-4686(92)85026-H.
[22] Y. Watanabe, K. Nakamura, N. Kobayashi, Electrochromic properties of the polyethylene terephthalate derivative film-modified electrode, Polym. Adv. Technol. 22 (2011) 1283–1285, https://doi.org/10.1002/pat.2003.
[23] T. Fu, C. Zhao, Y. Zhu, P. Zhang, Y. He, H. Meng, Towards the design of ideal electrochromic materials with low driving voltage based on phthalate derivatives, Org. Electron. 95 (2021) 106189, https://doi.org/10.1016/j.orgel.2021.106189.
[24] T.J. Adams, A.R. Brotherton, J.A. Molai, N. Parmar, J.R. Palmer, K.A. Sandor, M. G. Walter, Obtaining reversible, high contrast electrochromism, electrofluorochromism, and photochromism in an aqueous hydrogel device using chromogenic thiazolothiazoles, Adv. Funct. Mater. 31 (2021) 2103408, https://doi.org/10.1002/adfm.202103408.
[25] R. Hayes, G.G. Warr, R. Atkin, Structure and nanostructure in ionic liquids, Chem. Rev. 115 (2015) 6357–6426, https://doi.org/10.1021/cr500411q.
[26] N.V. Plechkova, K.R. Seddon, Applications of ionic liquids in the chemical industry, Chem. Soc. Rev. 37 (2008) 123–150, https://doi.org/10.1039/b006677j.
[27] D.D. Patel, J.M. Lee, Applications of ionic liquids, Chem. Record 12 (2012) 329–355, https://doi.org/10.1002/tcr.201100036.
[28] C.C. Yan, W. Li, Z. Liu, S. Zheng, Y. Hu, Y. Zhou, J. Guo, X. Ou, Q. Li, J. Yu, L. Li, M. Yang, Q. Liu, F. Yan, Ionogels: preparation, properties and applications, Adv. Funct. Mater. (2023), https://doi.org/10.1002/adfm.202314408.
[29] X. Fan, S. Liu, Z. Jia, J.J. Koh, J.C.C. Yeo, C.G. Wang, N.E. Surat'man, X.J. Loh, J. Le Bideau, C. He, Z. Li, T.P. Loh, Ionogels: recent advances in design, material properties and emerging biomedical applications, Chem. Soc. Rev. 52 (2023) 2497–2527, https://doi.org/10.1039/d2cs00652a.
[30] Z. Luo, W. Li, J. Yan, J. Sun, Roles of ionic liquids in adjusting nature of ionogels: A mini review, Adv. Funct. Mater. 32 (2022) 2203988, https://doi.org/10.1002/adfm.202203988.
[31] J.Le Bideau, L. Viau, A. Vioux, Ionogels, ionic liquid based hybrid materials, Chem. Soc. Rev. 40 (2011) 907–925, https://doi.org/10.1039/c0cs00059k.
[32] B. Wang, W. Zhang, F. Zhao, W.W. Yu, A.Y. Elezzabi, L. Liu, H. Li, An overview of recent progress in the development of flexible electrochromic devices, Nano Mater. Sci. 5 (2023) 369–391, https://doi.org/10.1016/j.nanoms.2022.08.002.
[33] S.A. Sapp, G.A. Sotzing, J.R. Reynolds, High contrast ratio and fast-switching dual polymer electrochromic devices, Chem. Mater. 10 (1998) 2101–2108, https://doi.org/10.1021/cm9801237.
[34] Y. Alesanco, A. Viñuales, J. Rodriguez, R. Tena-Zaera, All-in-one gel-based electrochromic devices: strengths and recent developments, Materials, (Basel) 11 (2018) 414, https://doi.org/10.3390/ma11030414.
[35] I. Reche, I. Gallardo, G. Guirado, The role of cations in the reduction of 9-fluorenone in bis(trifluoromethylsulfonyl)imide room temperature ionic liquids, J. Chem. 38 (2014) 5030–5036, https://doi.org/10.1039/c4nj01200c.
[36] I. Reche, I. Gallardo, G. Guirado, An analysis of anion-specific effects on the standard potential shifts of 9-fluorenone in room-temperature ionic liquids with a silver electrode as a cathode material, ChemElectroChem. 1 (2014) 2104–2109, https://doi.org/10.1002/celc.201402243.
[37] F. Philippi, T. Welton, Targeted modifications in ionic liquids - from understanding to design, Phys. Chem. Chem. Phys. 23 (2021) 6993–7021, https://doi.org/10.1039/d1cp00216c.
[38] B. Wang, L. Qin, T. Mu, Z. Xue, G. Gao, Are ionic liquids chemically stable? Chem. Rev. 117 (2017) 7113–7131, https://doi.org/10.1021/acs.chemrev.6b00594.
[39] P. Xu, H. Chen, X. Zhou, H. Xiang, Gel polymer electrolyte based on PVDF-HFP matrix composited with rGO-PEG-NH2 for high-performance lithium ion battery, J. Memb. Sci. 617 (2021) 118660, https://doi.org/10.1016/j.memsci.2020.118660.
[40] S. Santiago, X. Muñoz-Berbel, G. Guirado, Study of P(VDF-co-HFP)-ionic liquid based ionogels for designing flexible displays, J. Mol. Liq. 318 (2020) 114033, https://doi.org/10.1016/j.molliq.2020.114033.
[41] S. Santiago, P. Giménez-Gómez, X. Muñoz-Berbel, J. Hernando, G. Guirado, Solid multiresponsive materials based on nitrospiropyran-doped ionogels, ACS. Appl. Mater. Interfaces. 13 (2021) 26461–26471, https://doi.org/10.1021/acsami.1c04159.
[42] Y. Watanabe, K. Imaizumi, K. Nakamura, N. Kobayashi, Effect of counter electrode reaction on coloration properties of phthalate-based electrochromic cell, Sol. Energy Mater. Sol. Cells 99 (2012) 88–94, https://doi.org/10.1016/j.solmat.2011.06.020.
[43] L. Wylie, K. Hakatayama-Sato, C. Go, K. Oyaizu, E.I. Izgorodina, Electrochemical characterization and thermodynamic analysis of TEMPO derivatives in ionic liquids, Phys. Chem. Chem. Phys. 23 (2021) 10205–10217, https://doi.org/10.1039/d0cp05350c.
[44] S.X. Deng, Y.H. Li, P. fei Cai, C.Y. Wang, H. Wang, Y.J. Shen, Electropolymerizations and electrochromic performances of tetrathiafulvalene-σ-thiophenes, poly, Bulletin 78 (2021) 5953–5961, https://doi.org/10.1007/s00289-020-03410-1.
[45] X. Luo, R. Wan, Z. Zhang, M. Song, L. Yan, J. Xu, H. Yang, B. Lu, 3D-Printed hydrogel-based flexible electrochromic device for wearable displays, Adv. Sci. 11 (2024) 2404679, https://doi.org/10.1002/advs.202404679.
[46] Y. Watanabe, T. Nagashima, N. Kobayashi, Spectro-electrochemical properties of phthalate derivative-based electrochromic cell with gel electrolyte containing DMSO solvent, Electrochem 77 (2009) 306–308, https://doi.org/10.5796/electrochemistry.77.306.